15. Mahyco, Baseline susceptibility of *Leucinodes orbonalis* Guen. populations to the Cry1Ac protein, 2006; http://www.envfor.nic.in/divisions/csurv/geac/bt_brinjal.html
16. Anon., AVRDC Report, Asian Vegetable Research Development Centre, Taiwan, 1998, p. 148.
17. Rao, N. G. V., Majumdar, A., Mandaokar, A. D., Nimbalkar, S. A. and Ananda Kumar, P., Susceptibility of brinjal shoot and fruit borer to the δ-endotoxins of *Bacillus thuringiensis*. *Curr. Sci*., 1999, **7**, 367–378.
18. Jalali, S. K., Lalitha, Y., Kamath, S. P., Mohan, K. S. and Head, G. P., Baseline sensitivity of lepidopteran corn pests in India to Cry1Ab insecticidal protein of *Bacillus thuringiensis*. *Pest Manage. Sci*., 2010, **66**, 809–815.
19. Hanur, V. S., *Bt* resistance and monophagous pests: handling with prudence. *Curr. Sci*., 2008, **95**, 449–451.
20. Hanur, V. S., In *Advances in Horticultural Biotechnology, Vol. I* (eds Singh, H. P., Parthasarathy, V. A. and Nirmal Babu, K.), Westville Publishing House, New Delhi, 2010, pp. 53–72.
21. Naranjo, S. E., Ruberson, J. R., Sharma, H. C., Wilson, L. and Wu, K., The present and future role of insect-resistant genetically modified cotton in IPM. In *Integration of Insect-Resistant, Genetically Modified Crops within IPM Programs* (eds Romeis, J., Shelton, A. M. and Kennedy, G. G.), Springer, Dordrecht, The Netherlands, 2008, pp. 159–194.

ACKNOWLEDGEMENTS. We are grateful to MRC, Bangalore, for providing the Cry1Ac protein and Directorate of UAS, Raichur for project sponsorship and financial support.

Received 29 March 2012; revised accepted 28 May 2013

Deccan Traps-associated obsidian glass: a nuclear waste containment

Nishi Rani[1], J. P. Shrivastava[1,*] and R. K. Bajpai[2]

[1]Department of Geology, University of Delhi, Delhi 110 007, India
[2]BETDD, Nuclear Recycle Group, Bhabha Atomic Research Centre, Mumbai 400 008, India

Alteration of obsidian collected from Osham Hill, Gujarat after treatment under hydrothermal-like conditions is compared with the naturally altered obsidian for its assessment as a nuclear waste glass. Experimental data have been obtained for ionic release, glass alteration and its retention in the residue. Geochemical evolution of obsidian shows partial to complete leaching of all the ions, but profusely of Si and Na ions. The ionic release is found in the order of Na > Si > K > Ca > Al = Mg > Fe > Mn > Ti. SEM-BSE images show distinct microstructures of smectite, montmorillonite and illite inside as well as outside the secondary layers, resulting from paragenesis of alteration products at various temperatures (100–300°C) and pressures (50, 250 and 1260 psi). It has been found that the octahedral cation occupancies of smectite are consistent with the dioctahedral smectite. The secondary layer composition shows retention for Si, Al and Mg ions, indicating their fixation in the alteration products, but remarkably high retention of Ti, Mn and Fe ions suggests release of a very small fraction of these elements into the solution. Devitrification of glass along the cracks, formation of spherulite-like structures, yellowish-brown palagonite, chlorite, calcite, zeolite and finally white-coloured clays that yielded after experiments, largely correspond to the minerals which are found in the residual soil profile (developed over fresh obsidian outcrops), formed as a result of weathering in the natural environment.

Keywords: Clay mineralogy, microtexture, neo-formed minerals, obsidian.

THE process of vitrification involves assimilation of nuclear waste into high-silica glass to develop a corrosion-resistant and highly durable matrix for its safe disposal in the geological repository. The heat generated due to decay of stored radionuclide raises the temperature; thus, hydrothermal-like conditions form within the glass matrix which causes release of radionuclide into the surrounding medium[1]. Prediction of glass dissolution rate on long-term basis requires an understanding of glass and environmental reactions[2]. In order to establish alteration mechanism and mineral paragenesis by inducing alteration in glass under hydrothermal-like conditions, Shrivastava *et al.*[3] discussed chemico-mineralogical attributes of surface layers and alteration products. Basaltic glass is considered as a natural analogue for the evaluation of the long-term stability of the nuclear waste[4]. However, good quality of obsidian that occurs in Osham Hill, Gujarat, India[5] is also considered as a potential natural analogue for long term stability of nuclear waste. In contrast to several studies focused on dissolution rate of basaltic and borosilicate glasses, corresponding studies on acid volcanic glasses (such as obsidian, rhyolite and impact glasses) are rare. Liritzis and Laskaris[6] used hydration rim and diffusion profiles to determine diffusion rates and mechanism as formed by hydration/diffusion during alterations in obsidian. However, complexity of phases due to variability in the properties is noted in case of obsidian collected from different locations[6]. To address these issues and to understand the chemico-mineralogical changes that occur at or near the surface, the present experimental study on obsidian was performed under hydrothermal-like conditions. Alteration mechanism is studied to assess its performance in the geological repository under hydrothermal-like conditions as sufficient water and radioactive heat is available in the system. The induced microtextural and mineralogical changes have

*For correspondence. (e-mail: jpshrivastava.du@gmail.com)

been compared with the obsidian which has undergone weathering in a natural environment after its formation (~ 65 Ma).

The Deccan Traps in India – a continental flood basalt province that records immense accumulation of tholeiitic lavas, erupted in a short timespan (~ 0.5 Ma)[7]. However, Chenet *et al.*[8,9] have proposed a relatively longer duration (64.7–68.5 Ma) for its volcanic activity, encompassing the Cretaceous/Palaeogene boundary (65–65.5 Ma)[10]. Felsic volcanism is associated with the closing phase of the Deccan volcanic episode. Felsic volcanic rocks are represented in Osham, Girnar, Alech and Barda Hills and Kutch in Gujarat. In Osham, the present study area (70°15′0″–70°17′30″E and 21°32′30″–21°34′10″N), a circular outcrop is exposed covering an area of approximately 6 km^2. The area comprises of rhyolite with obsidian flows at the base of the hill close to its contact with horizontal basalt lava flow. Brecciated rhyolite is also present. Deccan basaltic flows at the foot of the hill carry secondary quartz, zeolite and calcite, which often fill the open spaces in the rock. The acid volcanic rocks occur in the central and southeastern parts of Osham Hill, where minor flows contain 2–5 m thick obsidian lenses. Obsidian flows are separated by rhyolite from the basalt lava flows. Obsidian glass of this area is translucent, pitch black in colour and shows vitreous lustre. It is often banded and shows conchoidal fractures. Minor folds, prominent joints and fractures are also present. Glass, spherulite and feldspar can be seen in the obsidian. The rock contains abundant and also rounded to polygonal spherulites containing tiny (0.003 mm) feldspar grains. The Deccan Traps unconformably overlie Dharangdhara Formation of the Cretaceous, comprising bedded gritty arkose. Majority of lava flows are compound lava flows. Flow units show chilled bottom, pipe amygdales (quartz, calcite and zeolite) and vesicular top, similar to those found in the eastern Deccan volcanic province[11]. In a pile of 13 lava flows, 9 flows are 'pahoehoe' type, the rest show character of 'aa' type lavas similar to those reported from Mandla lobe[12].

For characterization, the obsidian sample was powdered in a ball mill to –200 μm mesh size. The sample is characterized by 7.11% LoI. Major oxide composition is SiO_2 = 69.50, TiO_2 = 0.18, Al_2O_3 = 12.00, $Fe_2O_3^{(total)}$ = 2.63, MnO = 0.05, MgO = 0.07, Na_2O = 3.50, K_2O = 3.71, P_2O_5 = 0.03. Total alkali–silica plot confirms rhyolitic composition[13]. To achieve optimum *S*/*V* (surface area/volume) value for the test glass, obsidian chips were pulverized and sieved to obtain 100–120 μm particles. Glass specimens were ultrasonically cleaned repeatedly in deionized water and acetone and allowed to dry at 90°C for 24 h. The specific area and density of specimen measured by BET (Krypton) method were 663 cm^2/g and 2.405 g/cm^3 respectively. Thirty-four sets of experiment were performed in the Parr reactor, where each 1.0 g of glass specimen was treated with 80 ml of deionized water at 100°C, 150°C, 200°C and 300°C temperature and 50, 250 and 1260 psi pressures respectively for 1, 2, 4, 8, 16, 32, 64, 128 and 256 h. Prior to analysis of leachates, pH and conductivity measurements were done at room temperature (25°C). Leachates were analysed using ICP-MS to determine ionic release of Si, Al, Mg, K, Ca, Ti, Fe and Mn. XRD and SEM–EDS analyses were carried out to understand form, structure and composition of the residue and they were compared with the naturally weathered obsidian outcrops. Intrinsic water is the dominant factor while ascertaining the rate of hydration. It shows strong positive correlation with the hydration rate. However, later is possibly related to the depolymerizing effect of intrinsic water, possibly OH^- in the glass structure[13]. Thus, homogeneity of obsidian with respect to intrinsic water content is assessed for obsidian as it varies within a single flow. Intrinsic water includes hydroxyl (OH^-) and molecular water (H_2O) and these are measured by infrared (IR) spectroscopy[14]. IR spectra (Figure 1) of the untreated specimen show a broad asymmetric band that peaks at ~ 3570 cm^{-1}, attributed to OH stretching vibration, whereas H_2O is identified by a symmetrical band at ~ 1630 cm^{-1}, which is due to the bending of H_2O molecules[14]. Intrinsic water determined for obsidian (Figure 1) is ~ 1.12 wt%. Diffusion of water inwards into the glass is a significant factor which facilitates mobilization of diffused species and therefore helps to ascertain the rate of diffusion and reaction kinetics in the diffused layer. To understand distribution, concentration and activity of chemical species in an aqueous system, glass composition was simulated using the EQ3/6 software package[15]. It has been found that the solution becomes saturated with one or more minerals at any stage of progress of the reaction;

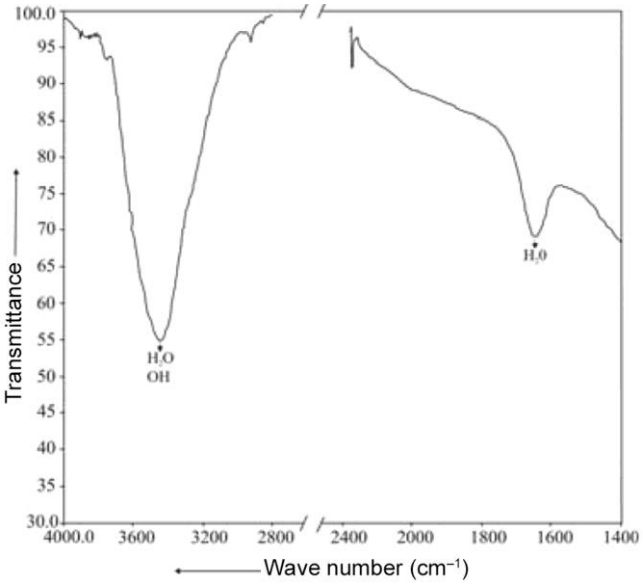

Figure 1. IR spectra (4000–1400 cm^{-1}) of untreated specimen showing broad, asymmetric bands of OH and H_2O at ~ 3570 and ~ 1630 cm^{-1} vibrations respectively.

the activities and molalities of all the aqueous species together with the number of moles of each mineral produced and destroyed during the reaction progress were computed as a function of time. Based on glass dissolution equations, reaction progress is plotted against saturation index (log Q/K), which shows saturation with respect to solid phase. Several factors contribute to the nucleation and growth of a secondary phase, including kinetic constraints on precipitation[16].

When obsidian glass specimen is treated for 64 h at 300°C, the pH and conductivity of the leachate show high values. To quantify mass loss (ML), the mass of each specimen was measured (before and after each experiment) and elemental release rates (mmol/l and NLi (normalized mass loss)) for Si, Na, Al, Mg, K, Ca, Ti, Fe and Mn were calculated (sensitivity of ML = 0.01%). ML, NLi and rate of dissolution (g/m^{2}d) of glass as a function of time are plotted in Figure 2. It can be seen that there is an increase in the glass alteration with the rise in the temperature. Alteration peaks are observed at low as well as high temperatures. The elemental release rates and ML show identical behaviour. The process of hydrolysis dominates glass alteration rate at pH < 9, but ion-exchange controls the reactions at pH > 9. Precipitation

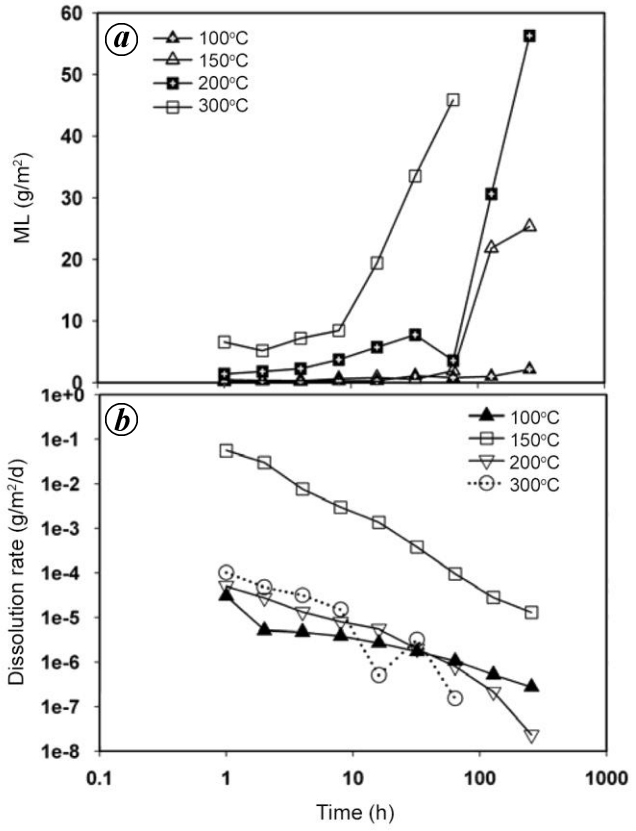

Figure 2. Data plotted for (***a***) time versus mass loss [ML (g/m^2)], and (***b***) dissolution rates as a function of alteration for obsidian glass, treated under hydrothermal-like conditions at 100°C, 150°C, 200°C and 300°C.

reactions play an important role under saturated conditions for long-term performance, whereas ion exchange and network hydrolysis are the dominant processes for short-term conditions[17]. In case of obsidian, the former dominates initially between 100°C and 150°C. Therefore, the glass alteration rate is enhanced with time, whereas at relatively higher (200°C and 300°C) temperatures, glass alteration gets stabilized and remains more or less constant with time. High alteration rate is due to the effect of the solution composition. As elemental concentration increases in the leachate, the elemental release rate generally decreases[18], thus indicating large-scale breaking of the glass network. As a result, more glass dissolution takes place in the initial stage of the reaction. High Na release in water leads to weakening of the network structure; therefore, subsequently it is more readily attacked by water. The elevated participation of ion exchange process, particularly when the S/V ratio of the test sample is high, causes overall release of elements which is possibly responsible for the increase in the pH of the leachates[19]. The initial reaction causing alkali release, resulted from water diffusion into the glass network. As the release rate decreases with the increasing depth of alkali depletion in the outer glass surface, matrix dissolution becomes the dominant process. Data on time of alteration (h) and elemental release when plotted show meagre release rate for Fe and Mn (except for Ti) at low temperature. But, at higher temperature, these elements show high release rate. Very low release is represented by Al, Mg and Ca, but high release of K is noticed at all temperatures. The normalized mass loss of released glass constituents (Na and Si) shows high glass dissolution rate (Figure 3). In Figure 3, release of constituent elements (Ti, Fe and Mn) from glass, calculated as NLi is plotted against time. It can be seen that there is preferential release of Fe compared to Ti and Mn. NLi plot for Al, Mg, K and Ca shows high release of Ca relative to Al, Mg and K (Figure 3). It has been found that the dissolution drops down to a constant rate at the stage of Si saturation. The ionic release is in the order Na > Si > K > Ca > Al = Mg > Fe > Mn > Ti. Alteration layer formed during under-saturated condition is highly porous and has no protective properties[20]. If silica attains saturation, the dissolution rate drops down by several orders of magnitude due to precipitation and sorption of the hydrolysed species. A dense, highly protective silicate layer develops on the glass surface, forming a diffusion barrier that limits the diffusion of water into the gel[21]. After saturation, glass dissolves with a low but constant rate. The slower Si dissolution is explained by the sorption of added metal ions onto the gel layer of the glass, therefore, silica saturation is attained after much longer times. The low Si concentration after precipitation also represents a saturation concentration with respect to a glass surface layer developed by precipitation or sorption of silicate phases. In all the solutions studied, the dissolution rate drops down at Si saturation to the same

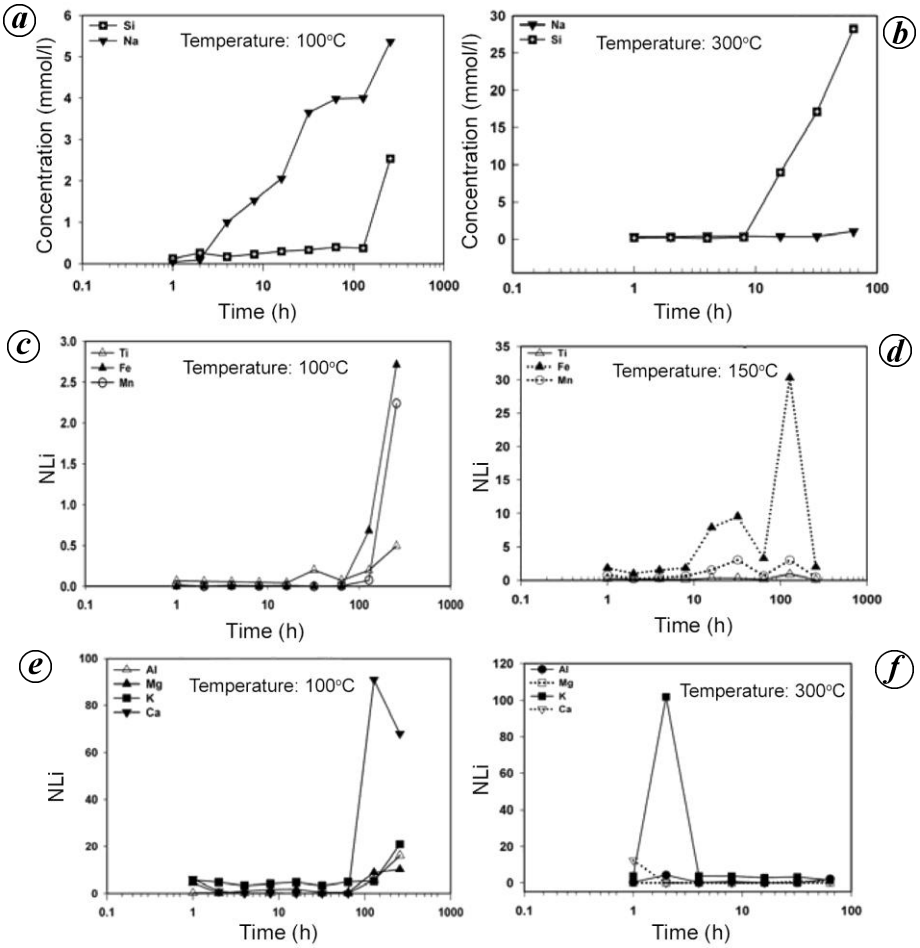

Figure 3. Plots for time versus release rate (mmol/l) for Si and Na at (***a***) 100°C and (***b***) 300°C; for Ti, Fe and Mn at (***c***) 100°C and (***d***) 150°C; for Al, Mg, K and Ca at (***e***) 100°C and (***f***) 300°C.

low constant rate. With the rise in the pH value, the diffusion coefficient of water into the glass surface decreases and correspondingly the constant dissolution rate[22]. By ageing of gel and retention of less soluble elements, the barrier effect of the gel layer increases, thus, initial constant release rate begins to diminish slowly with the progression of time.

When amorphous, black coloured obsidian glass (Figure 4 *a*) is treated under hydrothermal-like conditions (at 100°C, 150°C, 200°C and 300°C temperature and 50, 120, 250 and 1260 psi pressure, respectively), widespread decomposition of glass and formation of secondary clays is noticed over the surface and outside the spherical glass structure (Figure 4 *b*). Altered obsidian grain surface shows abundant neo-formed minerals with two distinct morphologies: (i) massive aggregate (Figure 4 *b*) and (ii) platy flakes along with a series of channels and cusps similar to that found in smectite (Figure 4 *c*). Transformation of glass into neo-formed mineral is observed (Figure 4 *d*). The form of equidimensional grains is typical of smectite, which consists of clay-like flakes forming rosette-like particles (Figure 4 *e*). Isolated particles present over the glass surface, form large aggregates. Curved clay-like material occurs on the surface, enveloping grains and forms mosaic texture (Figure 4 *f*). The Na, Si and Ca concentrations increased regularly and remain almost constant in case of specimen treated for 64 h, whereas Si and Al concentrations remained constant after 32 h. The Al, Fe and Ti contents were found strongly retained. Clay compositions of altered specimens when plotted in SiO_2–Al_2O_3–Fe_2O_3 and SiO_2–Al_2O_3–CaO ternary diagrams (Figure 5) and compared with the standard clays[22], indicate that the clays derived from the alteration of obsidian are chiefly composed of Al, Na and Fe, which have led to the formation of montmorillonite, illite and beidellite. Structural formulae (Table 1) of clay minerals were calculated on half unit cell basis, consisting of 22 negative charges [$O_{10}(OH)_2$]. They indicate that the octahedral cation occupancies in the neo-formed smectite are more or less similar to those reported by Ransom and Helgeson[23] for dioctahedral smectites. The chemical composition of the residue is close to that of smectite and resulting formula resembles that of the dioctahedral smectite. The octahedral and inter-layer charges

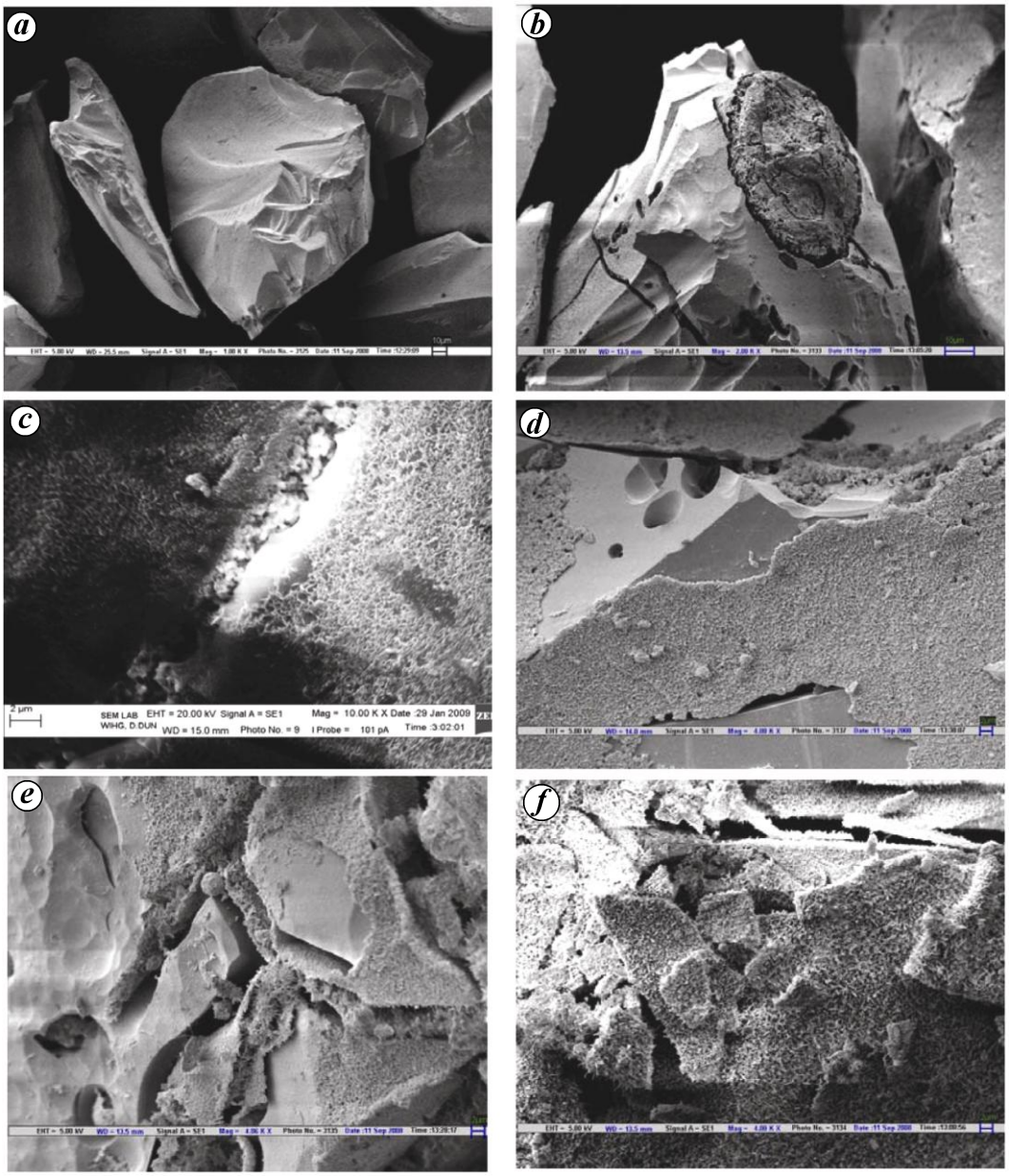

Figure 4. SEM–BSE images of obsidian: ***a***, Untreated specimen; ***b***, Treated specimen at different temperatures and time showing boundary where certain amount of dissolution is noticed in the middle of the glass particles; ***c***, Glass surfaces clustered to form massive aggregates; cellular honeycomb structure indicates presence of smectite; ***d***, Two distinct morphologies of glass; ***e***, Partially transformed glass into crystalline material; ***f***, Complete transformation of glass into crystalline phase.

of the neo-formed smectites as resulted from the solid-state rearrangement of hydrated external layer was calculated. Ionic retention[24] is calculated from the measured molar concentrations and composition of unaltered glass by normalizing to congruently dissolved elements. During glass alteration, waste constituents participate in the formation of crystalline products on the glass surface and become part of their structure. When SiO_2 versus (a) K_2O and (b) Na_2O data for all the treated glass specimens are plotted in bivariate diagrams (Figure 6), they indicate that the plots lie well within the compositional limits of a clay zone, thus, indicating the formation of clays at the end the alteration reaction. Al, Si, Na, Ca and Al are released incongruently. Therefore, ionic retention also indicates composition of gel derived from obsidian. It contains high amounts of Si, Al and Mg, which indicate fixation of these elements in the alteration products. These findings correlate well with the compositions obtained by Energy Dispersive Spectroscopy (EDS) (Table 1), which revealed formation of abundant Al, Ca and Fe alumino-silicates.

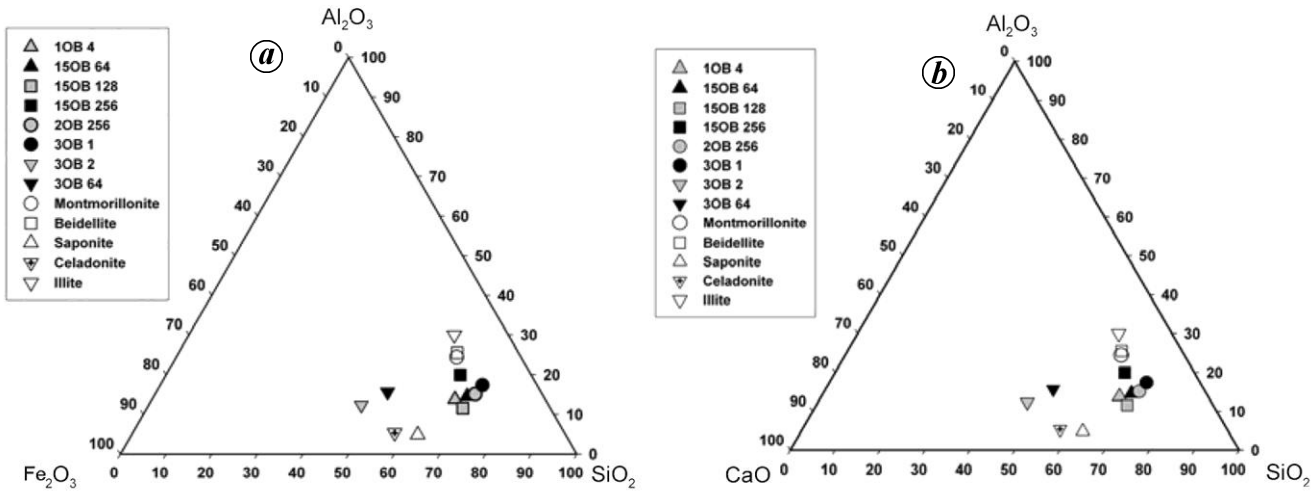

Figure 5. Compositional data (wt%) for treated specimens plotted over (***a***) Al_2O_3–Fe_2O_3–SiO_2 and (***b***) Al_2O_3–CaO–SiO_2 ternary diagrams and compared with the published (Weaver and Pollard, 1973) values of clay. They show closeness with the montmorillonite and illite compositions.

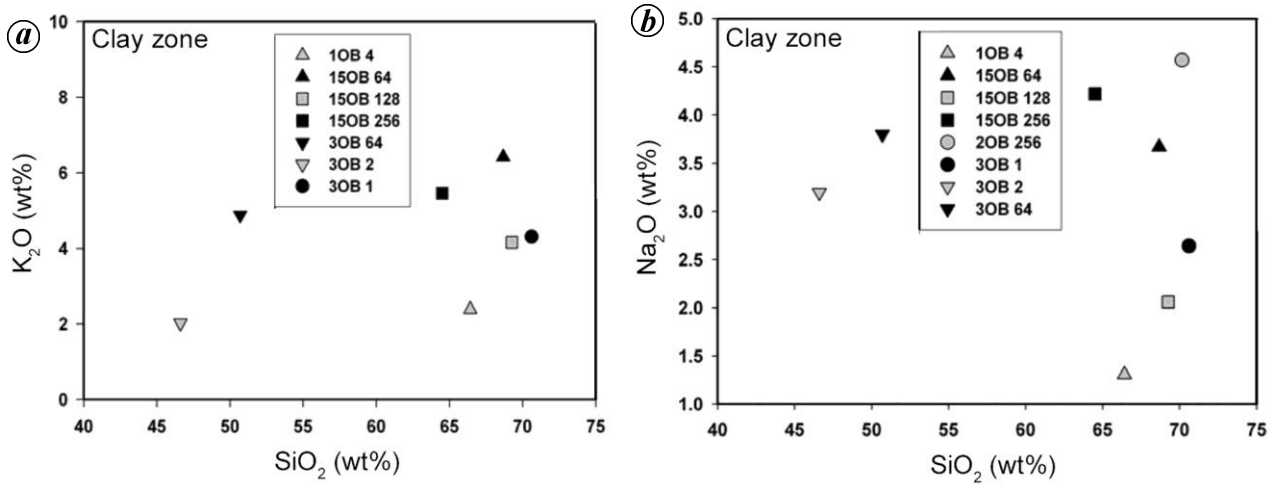

Figure 6. SiO_2 versus (***a***) K_2O and (***b***) Na_2O data plots for all the treated glass specimens which lie within the compositional limits of a clay zone showing formation of clays at the end the alteration reaction.

High retention of Ti, Fe and Mn signifies release of small fractions of these elements into leachates. In the gel layer, Al ions likely have fourfold and sixfold co-ordinations. The structure involves an excess of charges, thus requiring presence of compensators, such as alkaline and alkaline earth elements for charge balance. This view draws support from the explanation that glass with large amounts of Na, Al and Ca forms a gel layer, rich in Na that compensates for the AlO^{4-}. In obsidian alteration, gel layers contain significant amounts of Al, Na and Fe ions which on an average are equimolar (questionable), possibly corresponding to the compensation of AlO^{4-} charges by Na (ref. 25). At high temperatures, the glass layer contains very low amounts of Na, but it is high in Ca ions. One possible explanation for this is that the Ca ions behave like a main compensator for charge balance.

Glassy material is devitrified by alteration. Microcrystalline and spherulitic feldspar are formed. Specimens show yellow to dark brown stains, indicating glass alteration. Fresh obsidian outcrop over which less, moderately and intensely weathered crust has developed was also studied simultaneously and compared with the experimentally altered specimens. It has been found that pH of the solution, ionic release and glass-water (including intrinsic water) interface operative at hydrothermal-like conditions, play a significant role for microtextural and mineralogical changes both in the experimentally altered as well as naturally altered obsidian. Petrography revealed the presence of yellowish-brown palagonite, chlorite, calcite, zeolite and smectite from less to intensely weathered profile (Figure 7). Short-term alteration studies at low temperature show the presence of palagonite – the initial

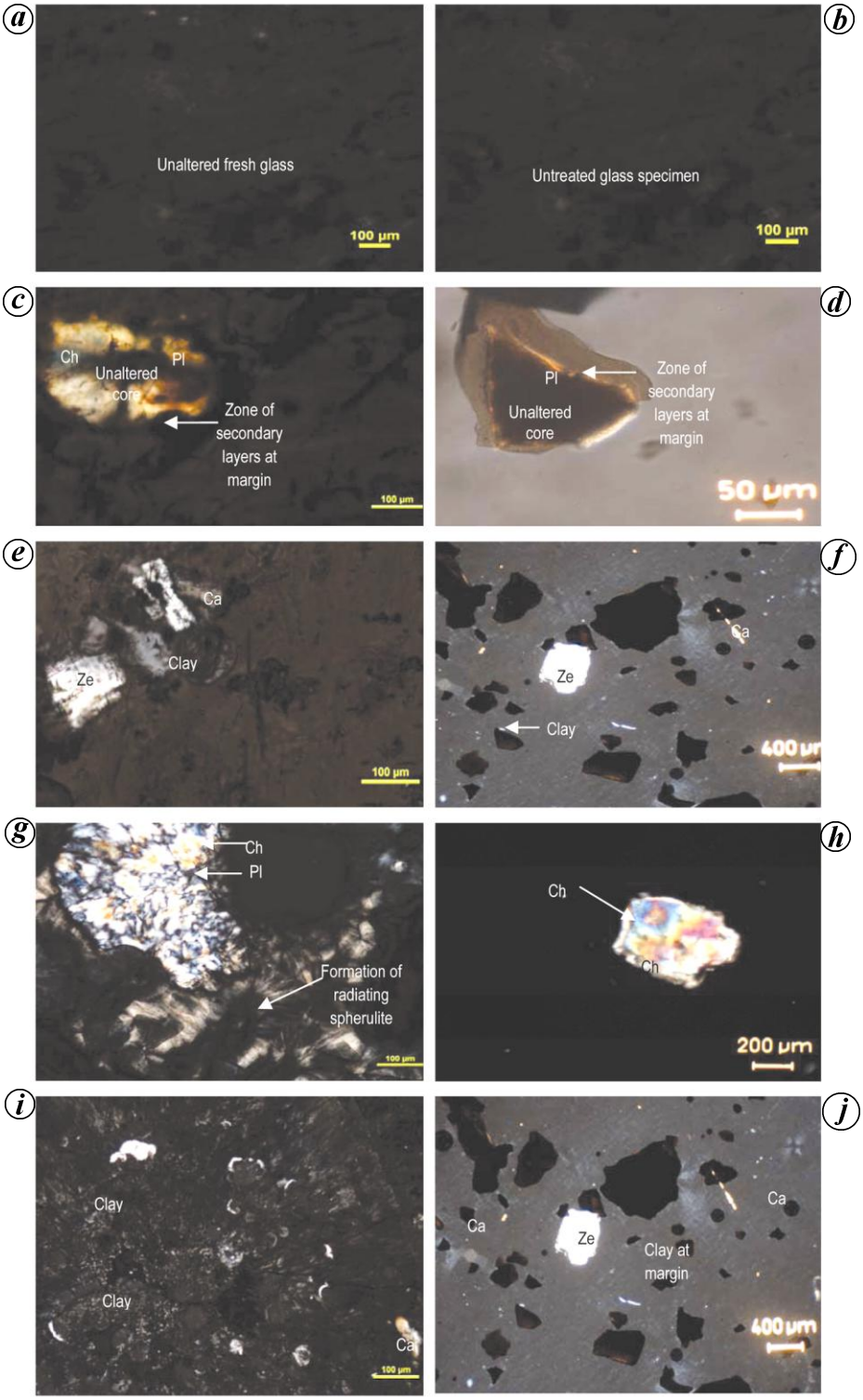

Figure 7. Photomicrographs for comparison of naturally weathered (left-hand side) and treated (right-hand side) obsidian for 256 h under hydrothermal-like conditions. ***a***, Amorphous, black coloured, unaltered obsidian from Osham Hill; ***b***, Untreated glass specimen devoid of crystalline phase; ***c***, Least weathered glass in natural environment, containing crystalline brownish-yellow palagonite (Pl) and green-coloured chlorite (ch) surrounding unaltered glassy core; ***d***, Secondary layer of brownish-yellow palagonite (Pl), developed around glassy core treated at 100°C; ***e***, Appearance of calcite (Ca), zeolite (Ze) and small amounts of clay in moderately weathered glass in natural environment; ***f***, Similar mineralogical assemblage as observed in moderately weathered glass treated at 150°C; ***g***, Development of needles, radiating spherulitic, crystalline, brownish-yellow palagonite (Pl) in highly weathered glass; ***h***, Resembles the mineral assemblage found in (***g***) with glass treated at 200°C, except for the presence of radiating crystalline phase. ***i***, Highly weathered glass represents fine-grained, scattered, white clay; ***j***, Presence of calcite (Ca), zeolite (Ze) and clay at the margin of the glass grain treated at 300°C.

Table 1. Layer charges and structural formulae of clay residues calculated using major oxide data (wt%) on a half unit cell basis, consisting of 22 negative charges $[O_{10}(OH)_2]$ for a selected group of neo-formed minerals formed by alteration of obsidian glass

Sample	1OB4	3OB 1	3OB2	3OB64	15-OB64	15-OB128	15-OB256	2-OB256
Na_2O (wt%)	1.13	3.67	2.06	4.22	4.57	2.37	2.63	3.37
MgO	–	–	0.62	–	–	–	–	–
Al_2O_3	10.22	14.59	11.54	19.93	15.13	13.33	8.63	11.80
SiO_2	47.28	68.67	69.26	64.50	70.15	51.98	31.32	36.69
K_2O	1.22	6.42	4.16	5.46	4.56	–	0.98	2.54
Fe_2O_3	0.61	6.64	12.36	5.89	5.59	1.00	0.69	2.34
CaO	1.50	–	–	–	–	0.75	0.49	1.46
Layer charge								
Tetrahedral								
Si	4.42	4.28	4.16	3.83	4.24	4.27	3.98	4.27
$Al^{(iv)}$	–0.42	–0.28	–0.16	0.17	–0.24	–0.27	0.02	–0.27
Octahedral								
$Al^{(vi)}$	1.50	1.52	1.48	1.23	1.30	1.11	1.42	1.36
Fe^{3+}	0.09	0.11	0.14	0.33	0.31	0.57	0.27	0.26
Mg	0.00	0.00	0.00	0.00	0.00	0.06	0.00	0.00
Interlayer								
Ca	0.21	0.09	0.10	0.23	0.00	0.00	0.00	0.00
Na	0.17	0.31	0.56	0.56	0.44	0.25	0.50	0.54
K	0.20	0.33	0.23	0.47	0.51	0.33	0.43	0.35

Sample	Structural formula	Morphology	*T*	*t*	OC
1OB4	$[Al_{1.5}Fe^{3+}_{.09}][Si_{4.42}Al_{-0.42}]O_{10}(OH)_2.Ca_{0.21}Na_{0.17}K_{0.2}$	Porous sponge-like structure	100	4	1.59
15-064	$[Al_{1.3}Fe^{3+}_{.31}][Si_{4.24}Al_{-0.24}]O_{10}(OH)_2.Ca_0Na_{0.44}K_{0.51}$	Channels with etch and pits	150	64	1.61
15-0128	$[Al_{1.11}Fe^{3+}_{.57}Mg_{0.06}][Si_{4.27}Al_{-0.27}]O_{10}(OH)_2.Ca_0Na_{0.25}K_{0.33}$	Globular secondary growth	150	128	1.68
15-0256	$[Al_{1.42}Fe^{3+}_{.27}][Si_{3.98}Al_{0.02}]O_{10}(OH)_2.Ca_0Na_{0.5}K_{0.43}$	Honeycomb-like structure	150	256	1.69
20-0256	$[Al_{1.36}Fe^{3+}_{.26}][Si_{4.27}Al_{-0.27}]O_{10}(OH)_2.Ca_0Na_{0.54}K_{0.35}$	Rosette-like particles	200	256	1.62
3OB1	$[Al_{1.52}Fe^{3+}_{.11}][Si_{4.28}Al_{-0.28}]O_{10}(OH)_2.Ca_{0.09}Na_{0.31}K_{0.33}$	Two distinct layers	300	1	1.63
3OB2	$[Al_{1.48}Fe^{3+}_{.14}][Si_{4.16}Al_{-0.16}]O_{10}(OH)_2.Ca_{0.1}Na_{0.56}K_{0.23}$	Cracks with distinct morphology	300	2	1.62
3OB64	$[Al_{1.23}Fe^{3+}_{.33}][Si_{3.83}Al_{0.17}]O_{10}(OH)_2.Ca_{0.23}Na_{0.56}K_{0.47}$	Spherulites scattered over the glass particle	300	64	1.56

*OC, Octahedral occupancy; *T*, Temperature (°C); *t*, Time (h).

product of volcanic glass alteration which is also found in less-weathered obsidian. It is formed by glass dissolution with the concomitant precipitation of insoluble residue at the glass–water interface. Ionic mobility is enhanced in the alteration experiments, causing depletion of Na > Si > K > Ca and enrichment of Al > Mg > Fe > Mn > Ti ions in the glass, resulting in the formation of palagonite.

The present study on microtextural framework and microchemistry of altered obsidian glass shows reliable evolutionary changes: (a) partial to complete leaching of all the ions, but profusely of Si and Na ions, and (b) growth of secondary phases such as palagonite, clay (smectite, illite and montmorillonite) and other minerals (calcite and zeolite). The process and extent of palagonitization in the initial stage and formation of smectite in the later stage of alteration in natural outcrops are comparable to the experimentally altered obsidian specimens. The mode of glass dissolution and the properties of secondary phases plays a significant role in ionic release rates. They are also critical in establishing the long-term alteration effects of obsidian glass, thus, suggesting its suitability as a natural analogue for long-term alteration of nuclear waste glass.

1. Ceelen, W., *et al.*, Caesium diffusion in sodium borosilicate glass studied by low-energy ion scattering. *Surf. Interface Anal.*, 1995, **23**, 712–716.
2. Small, J. S., Trivedi, D. P. and Abraitis, P. K., Modelling of glass dissolution and transport with the code SUGAR. *Mater. Res. Soc. Symp. Proc.*, 1998, **506**, 253.
3. Shrivastava, J. P., Bajpai, R. K. and Rani, N., A review on corrosion mechanism in borosilicate nuclear waste glass for long-term performances assessments in geological repository. *J. Geol. Soc. India*, 2008, **72**, 238–244.
4. Byers, C. D., Jercinovic, M. J., Ewing, R. C. and Keil, K., Basalt glass: an analogue for the evaluation of the long-term stability of the nuclear waste form borosilicate glasses. *Mater. Res. Soc. Symp. Proc.*, 1985, **44**, 583.
5. Rani, N., Shrivastava, J. P. and Bajpai, R. K., Obsidian: a potential natural analogue for nuclear waste glass. *Curr. Sci.*, 2010, **98**, 950–954.
6. Liritzis, I. and Laskaris, N., Fifty years of obsidian dating in archaeology. *J. Non-Cryst. Solids*, 2011, **357**, 2011–2023.
7. Courtillot, V. A., Volcanic eruption. *Sci. Am.*, 1990, **263**, 53–60.
8. Chenet, A.-L., Fluteau, F., Courtillot, V., Gerard, M. and Subbarao, K. V., Determination of rapid Deccan eruptions across the Cretaceous–Tertiary boundary using paleomagnetic secular variation: results from a 1200-m-thick section in the Mahabaleshwar escarpment. *J. Geophy. Res.*, 2008, **113**, doi:10.1029/2006JB004635.

9. Chenet, A.-L. *et al.*, Determination of rapid Deccan eruptions across the Cretaceous–Tertiary boundary using paleomagnetic secular variation: 2. Constraints from analysis of eight new sections and synthesis for a 3500-m-thick composite section. *J. Geophys. Res*., 2009, **114**, B06103; doi:10.1029/2008JB005644.
10. Gradstein, F. M., Ogg, J. G. and Smith, A. G., *A Geologic Time Scale*, Cambridge University Press, Cambridge, 2004, p. 589.
11. Kashyap, M., Shrivastava, J. P. and Raju Kumar, Occurrence of small scale inflated pahoehoe lava flows in the Mandla lobe of the eastern Deccan volcanic province. *Curr. Sci*., 2010, **98**, 72–76.
12. Patnayak, S. K. and Shrivastava, J. P., Petrography and major-oxide geochemistry of basalts from the eastern Deccan volcanic province, India. *Mem. Geol. Soc. India*, 1999, **43**, 233–270.
13. LeMaitre, R. W., A proposal by the IUGS sub-commission on the systematics of igneous rocks for a chemical classification of volcanic rocks based on the total alkali silica (TAS) diagram. *J. Petrol*., 1976, **17**, 589–637.
14. Stevenson, C. M., Knaus, Elizabeth, Mazer, J. J. and Bates, J. K., Homogeneity of water content in obsidian from the Coso Volcanic Field: implications for obsidian hydration dating. *Geoarchaeology*, 1993, **8**, 371–384.
15. Newman, S., Stopler, E. M. and Epstein, S., Measurement of water in rhyolitic glasses: calibration of an IR technique. *Am. Mineral*., 1986, **71**, 1527–1541.
16. Wolery, T. J., EQ3/6, a software package or geochemical modeling of aqueous systems, package overview and installation guide (version 7.0). Lawrence Livermore National Laboratory, USA, 1992.
17. McGrail, B. P., Ebert, W. L., Bakel, A. J. and Peeler, D. K., Measurement of kinetic rate law parameters on a Na ± Ca ± Al borosilicate glass for low-activity waste. *J. Nucl. Mater.*, 1997, **249**, 175–189.
18. Ebert, W. L., The effects of leachate pH and the ratio of glass surface area to leachant volume on glass reaction. *Phys. Chem. Glasses*, 1993, **34**, 58–65.
19. Neck, V., Fanghanel, Th. and Kim, J. I., Aquatische Chemie und Thermodynamische Modellierung von trivalenten Aktiniden, Forschungszentrum Karlsruhe, Report FZKA 6110, 1998.
20. Sheng, J., Shanggeng, L. and Tang, B., The leaching behaviour of borate waste glass SL-1. *Waste Manage*., 1999, **19**, 401–407.
21. Vernaz, E. and Gin, S. The apparent solubility of nuclear glasses, scientific basis for nuclear waste management. *Mater. Res. Soc. Symp. Proc.*, 2001, **XXIV**.
22. Grambow, B. and Muller, R. J., First order dissolution rate of surface layer in glass performance assessment law. *Nucl. Mater*., 2001, **298**, 112.
23. Ransom, B. and Helgeson, H. C., Compositional end-members and thermodynamic components of illite and dioctahedral aluminous smectite solid solutions. *Clays Clay Miner*., 1993, **41**, 37–550.
24. Curti, E., Crovisier, J. L., Morvan, G. and Karpoff, A. M., Long-term corrosion of two nuclear waste reference glasses (MW and SON68): a kinetic and mineral alteration study. *Appl. Geochem.*, 2006, **21**, 1152–1168.
25. Angeli, F., Charpentier, T., Gin, S. and Petit, J. C., O-17 3Q-MAS NMR characterization of a sodium aluminoborosilicate glass and its alteration gel. *Chem. Phys. Lett.*, 2001, **341**, 23–28.

ACKNOWLEDGEMENTS. N.R. thanks CSIR, New Delhi for providing financial assistance in the form of Research Associateship. We thank Activation Laboratories, Ontario for major oxide analysis and Dr P. P. Khanna, Dr N. K. Saini and Mr N. K. Juyal, WIHG, Dehradun, for ICP-MS and SEM-EDS.

Received 17 May 2012; revised accepted 17 April 2013

Effects of elevated water temperature on tolerance and stress in Chocolate mahseer *Neolissochilus hexagonolepis*: implications for habitat restoration and conservation

Sullip Kumar Majhi[1,2,*], Sanjay Kumar Das[1] and Dipjyoti Rajkhowa[1]

[1]ICAR Research Complex for North Eastern Hill Region, Umroi Road, Barapani 793 103, India
[2]ICAR Research Complex for Eastern Region, ICAR Parisar, P.O. B.V. College, Patna 800 014, India

The water temperature beyond tolerable limits adversely affects the growth and reproductive competence of teleost fish. The effect of such temperature rise will be more prominent in hill stream fishes like Chocolate mahseer because of their evolution in hilly environments and adaptation to low temperature. Here we examine the thermal tolerance, oxygen consumption and stress response in this fish species acclimatized at three different temperatures (24°C, 27°C and 30°C) for 45 days. The study reveals that CT_{max} and LT_{max} increased significantly ($P < 0.05$) with increasing acclimation temperature. Similarly, oxygen consumption rate at 24°C, 27°C and 30°C was 74.61 ± 2.11, 94.32 ± 2.33 and 122.54 ± 2.01 mg O_2 kg^{-1} h^{-1} respectively. Further, among the three acclimated temperatures tested, fishes reared at 24°C when subjected to thermal tolerance test encountered more stress (glucose level: 11.6 ± 1.14 mmol/l) than other groups (27°C: 9.22 ± 0.22 mmol/l; 30°C: 7.4 ± 0.89 mmol/l). Results suggest that water temperature of 31°C and beyond in natural water bodies of Meghalaya might create physiological stress in Chocolate mahseer, which in the long run may affect its reproductive performance. Therefore, we recommend adoption of proven *in situ* and *ex situ* conservation approaches to safeguard the species.

Keywords: Chocolate mahseer, climate change, thermal stress, teleost.

THE rising global temperature is receiving much attention because of its tremendous potential to disrupt ecosystems[1]. According to the latest reports, 'recent years have been among the warmest since 1860' and 'global mean temperature has increased by between 0.3°C and 0.6°C since the late nineteenth century'[1]. The increase of a few degrees in water temperature can set off ecological changes that would affect most forms of aquatic life. For example, fishes, as poikilotherm, are extremely sensitive to environmental changes and in particular to surrounding temperature. In general, temperature affects virtually all

*For correspondence. (e-mail: sullipkm@gmail.com)